HHS Public Access

Author manuscript

*J Bone Miner Metab*. Author manuscript; available in PMC 2018 July 01.

Published in final edited form as:

*J Bone Miner Metab*. 2017 July ; 35(4): 428–436. doi:10.1007/s00774-016-0796-1.

# Use of dual energy computed tomography to measure skeletal-wide marrow composition and cancellous bone mineral density

**Luke Arentsen, PhD**[1], **Karen E. Hansen, MD**[2], **Masashi Yagi, PhD**[3], **Yutaka Takahashi, PhD**[4], **Ryan Shanley, MS**[4], **Angela McArthur, MPH**[5], **Taiki Magome, PhD**[4], **Douglas Yee, MD**[4,6], **Jerry Froelich, MD**[7], and **Susanta Hui, PhD**[1,4,8]

[1]Department of Radiation Oncology, University of Minnesota, Minneapolis, MN

[2]Department of Medicine - Rheumatology, University of Wisconsin, Madison, WI

[3]Osaka University, Osaka, Japan

[4]Masonic Cancer Center, University of Minnesota, Minneapolis, MN

[5]Anatomy Bequest Program, University of Minnesota, Minneapolis, MN

[6]Department of Medicine, University of Minnesota, Minneapolis, MN

[7]Department of Radiology, University of Minnesota, Minneapolis, MN

[8]Department of Radiation Oncology, Beckman Research Institute, City of Hope, Duarte, CA

## Abstract

Temporal and spatial variations in bone marrow adipose tissue (MAT) can be indicative of several pathologies and confound current methods of assessing immediate changes in bone mineral remodeling. We present a novel dual energy computed tomography (DECT) method to monitor MAT and marrow corrected volumetric BMD (mcvBMD) throughout the body. Twenty-three cancellous skeletal sites in 20 adult female cadavers aged 40–80 years old were measured using DECT (80kVp and 140kVp). vBMD was simultaneous recorded using QCT. MAT was further sampled using MRI. Thirteen lumbar vertebrae were then excised from the MRI-imaged donors and examined by microCT.

After MAT correction throughout the skeleton, significant differences ($p < 0.05$) were found between QCT-derived vBMD and DECT-derived mcvBMD results. McvBMD was highly heterogeneous with a maximum at the posterior skull and minimum in the proximal humerus (574 mg/cc and 0.7 mg/cc, respectively). BV/TV and BMC have a nearly significant correlation with mcvBMD ($r = 0.545$, $p=0.057$ and $r = 0.539$, $p=0.061$, respectively). MAT assessed by DECT showed a significant correlation with MRI MAT results ($r = 0.881$, $p<0.0001$). Both DECT- and MRI-derived MAT had a significant influence on uncorrected vBMD ($r = −0.86$ and $r = −0.818$,

Address for correspondence: Susanta K Hui, PhD, DABR, Department of Radiation Oncology and Beckman Research Institute, City of Hope, 1500 E Duarte Rd, CA 91010, shui@coh.org.

**5.1. Conflicts of Interest**

Karen Hansen is a medical monitor and consultant to Deltanoid Pharmaceuticals. Luke Arentsen, Masashi Yagi, Yutaka Takahashi, Ryan Shanley, Angela McArthur, Taiki Magome, Douglas Yee, Jerry Froelich, and Susanta Hui declare no conflict of interest.

p≤0.0001, respectively). Conversely, mcvBMD had no correlation with DECT- or MRI- derived MAT (r = 0.261 and r = 0.067).

DECT can be used to assess MAT while simultaneously collecting mcvBMD values at each skeletal site. MAT is heterogeneous throughout the skeleton, highly variable, and should be accounted for in longitudinal mcvBMD studies. McvBMD accurately reflects the calcified tissue in cancellous bone.

**Keywords**

Whole-body imaging; marrow-corrected Bone Mineral Density; Dual Energy CT

## 1. Introduction

Cancellous bone can have sudden, drastic, and simultaneous changes in both calcified and marrow adipose tissue (MAT) [1, 2]. These changes can arise throughout the entire skeleton and be caused by a systemic stimulus or specific insult [3, 4]. Such responses are common from cytotoxic treatments such as radiation therapy and chemotherapy [5, 6]. MAT variations have recently been shown to indicate other skeletal and metabolic pathologies [7]. Scheller et al. have shown that in the mammalian skeleton, subsections of MAT can behave differently in response to a stimulus even within a single bone [8]. Identifing areas of global minima or comparing cancellous bone of different sites could highlight areas for further examination. Therefore, it is necessary to employ a modality that can accurately measure cancellous bone metrics throughout the entire body. Although the use of quantitative computed tomography (QCT) is useful to evaluate 3D cancellous bone, it has trouble comparing skeletal sites with significantly different bone marrow composition. For instance, hematopoietic bone marrow tissue has a higher linear attenuation coefficient than MAT. Therefore, sites with significant quantities of MAT compared to sites of hematopoietic tissue would show a lower vBMD, even if the same amount of mineralized tissue were present [9–12].

We have already shown dual energy computed tomography's (DECT) ability to simultaneously measure MAT quantities[13] and provide marrow corrected vBMD (mcvBMD) values that better reflect mineralized tissue [14]. Whole-body CT imaging is already commonly prescribed for the cancer patient for staging, treatment, and treatment follow-up (e.g. as part of a PET-CT procedure). DECT is feasible for clinical studies since, against conventional wisdom, doses from DECT have been shown to be similar to single energy CT [15, 16]. A quick, accurate, and efficient method to examine both MAT and marrow corrected vBMD would be beneficial to the cancer survivor [17]. The current study is the first to characterize both MAT and accurate vBMD of mineralized tissue throughout the whole body.

The primary goal of the current study is to accurately image the entire skeleton in order to characterize the heterogeneity of cancellous bone in terms of its bone mineral density and marrow composition (percentage of marrow space occupied by adipocytes). All aims were

conducted using 20 female cadavers, permitting excision of cancellous bone for *ex vivo* high resolution imaging.

## 2. Materials and Methods

### 2.1. Subjects

Approval for study was given by the University of Minnesota Anatomy Bequest program in accordance with the Minnesota Darlene Luther Revised Uniform Anatomical Gift Act. Over a 10 month period, twenty recently deceased human donors were accepted in the study. Women between the ages of 40 and 80 years old were selected to reduce confounding factors associated with gender and youth (e.g. unfused epiphyses) while still providing a range of marrow compositions. Donors were included if they were less than 190cm tall, had no history of anti-osteoporotic treatment, and could be imaged within 24 hours postmortem. The height restriction ensured that the body could fit within the longitudinal length of the CT scanner.

The mean (SD) age for all 20 subjects was 62 (13) years. The mean (SD) height and weight for subjects was 165cm (7cm) and 63kg (20kg), respectively, resulting in a BMI of 23.0 (6.4 $kg/m^2$). Causes of death included cancer (n=11), Parkinson Disease (n=2), chronic obstructive pulmonary disease (n=2), hepatitis (n=2), sudden cerebrovascular accident (n=2), and heart failure (n=1). One subject sustained a proximal femur fracture approximately one month before death but was never surgically treated, while another donor had prior bilateral knee replacement and shoulder reconstructive surgery. The high density material and resulting streak artifact made assessment of those regions unattainable in those two subjects. Any areas of obvious disease (e.g. metastases) or low signal-to-noise ratio were similarly avoided. In total, 14 of 460 sites were excluded from the analysis, mainly from the distal radius due to poor image quality (n=8).

### 2.2. Imaging

Within 20 hours of death, bodies were taken to the radiology department at the University of Minnesota Medical Center – Fairview for whole body dual energy CT scanning. Imaging was obtained using a Siemens® SOMATOM Definition Flash Dual Source CT scanner (Siemens Healthcare, Forchheim, Germany) at energies of 80kVp, 500mm SFOV, and 306–308mAs for Source A, and 140kVp, 328mm SFOV and 110–150mAs with a tin filter for Source B. During imaging, subjects were placed in a supine position with arms at the sides. The SOMATOM DECT unit was calibrated for both energies using the Mindways Software, Inc. (Mindways Software, Austin, TX, USA) QCTPro calibration Phantom. The table height was varied to ensure that the patient was in the center of the imaging field, regardless of body size. A calibration was performed for each table height.

### 2.3. Region of Interest analysis

Using anatomic landmarks and rigid registration software developed by Mindways Software, Inc. (Austin, Texas, USA), regions of interest (ROIs) were placed in the same location on the 80kVp and Sn140kVp CT scans. 446 cancellous bone locations between 20 donors were

analyzed (Fig. 1) including the skull, twelve sites from the spine, two from the arm, three from the hip, two from the knee, and three from the ankle/foot.

The size of each ROI depended on the bone being measured but ranged from a cylinder of 20 $mm^2$ × 3 mm for the posterior skull to 300 $mm^2$ × 9 mm for the lumbar spine (Fig. 2). Care was taken to exclude areas of prior fracture. ROIs were placed at each skeletal site for all donors and ROI sizes were recorded. Vertebrae were analyzed at the center of the vertebral body in the superior-inferior axis.

### 2.4. Basis Material Composition

To assess material composition of bone, a commercially available CT calibration phantom was included in each imaging procedure. The phantom was composed of five rods of different water and $K_2HPO_4$ concentrations (Mindways Software, Inc. Austin, TX) and placed underneath the lumbar spine and pelvis of the donor. Aqueous $K_2HPO_4$ is a commonly used physical standard for assessing bone mineral density (BMD). Relative to this standard, the basis material for bone as a function of BMD ($\rho_{K2HPO4}$) is described by the following relationship derived from conventional methods for estimating bone mineral density from single-energy CT data:

$$\rho_{H2O}(\rho_{K2HPO4}) = \rho_{H2O}(0) - 0.2174 \cdot \rho_{K2HPO4} \quad \text{(Equation 1)}$$

The factor of 0.2174 appearing in this equation describes how water is displaced from a fixed volume by way of addition of $K_2HPO_4$.

Using the publically available XCOM database to estimate energy-dependent, mass attenuation coefficients, we estimated the average atomic composition for basis materials ($\rho_{H2O}, \rho_{K2HPO4}$) [18]. We then employed the principle that when scanned with two different energies in the diagnostic range, the x-ray attenuation of biologic tissue can be described by the linear combination of the x-ray attenuation properties of $H_2O$ and $K_2HPO_4$ [19, 20]. We estimated the average basis material for identically placed ROIs in a phantom acquired at 80 kVp and 140 kVp using the following equations:

$$\rho_{H2O} = \frac{1}{D} \cdot [\beta_{K2HPO4,140} \cdot (CT_{80} - CT_{80}) - \beta_{K2HPO4,80} \cdot (CT_{140} - CT_{140})] \quad \text{(Equation 2)}$$

$$\rho_{K2HPO4} = \frac{1}{D} \cdot [\beta_{H2O,80} \cdot (CT_{140} - CT_{140}) - \beta_{H2O,140} \cdot (CT_{80} - CT_{80})] \quad \text{(Equation 3)}$$

$$D = \beta_{H2O,80} \cdot \beta_{K2HPO4,140} - \beta_{H2O,140} \cdot \beta_{K2HPO4,80} \quad \text{(Equation 4)}$$

where $CT_{80}$ and $CT_{140}$ were the average CT values within the defined ROIs and $\beta_{H2O,80}$, $\beta_{H2O,140}$, $\beta_{K2HPO4,80}$, $\beta_{K2HPO4,140}$ were calibration slopes determined from CT calibration phantom measurements.

The International Commission on Radiation Units and Measures has documented average atomic compositions of adipose tissue, yellow and red marrow (0.91 g/cm3, 0.93 g/cm3, and 1.03g/cm3, respectively)[21]. When combined with XCOM [18], these values were used as a reference range for the basis material compositions in our ROIs. This information, along with the aqueous $K_2HPO_4$ bone density standard described earlier was used to define a window of viable bone density estimates spanning a range of marrow compositions from 0% to 100% MAT. The porosity for this bone model is defined relative to the aqueous $K_2HPO_4$ bone density standard with 0 mg/cm$^3$ bone density on this scale assumed to correspond to a porosity of 1 and 1200 mg/cm$^3$ bone density assumed to correspond to a porosity of 0.

This technique of marrow composition estimation has been validated by a previous study [13]. Bone marrow composition and mcvBMD values were then estimated at each skeletal site using calibration slopes calculated for the whole body, similar to our previous investigation [14].

### 2.5. MRI analysis

In order to validate MAT assessment by DECT, immediately following DECT imaging, five random donors without history of fracture or prosthesis were scanned with Siemens MRI for marrow validation as previously described [22]. These donors were 47, 53, 54, 62, and 68 years old with a BMI of 20.7, 22.9, 22.1, 22.8, and 23.5, respectively. Briefly, after DECT imaging, the donor was imaged on a 3 Tesla MRI scanner (Tim TRIO, Siemens Medical Solutions, Malvern, PA, USA) using a three-point Dixon technique. Images were acquired in the supine position using the vendor's spine array receive coil combined with an anterior body matrix coil centered over the lumbar spine. After localizer scans, a series of 3D gradient echo images were acquired with TR = 9 microseconds, flip = 1°, matrix 448×266, 256 slices, 1.5 mm slice thickness, acquisition time 225 seconds. Three consecutive images were acquired with TE = 2, 3, and 4 microseconds. The raw image data were reconstructed offline in Matlab (MathWorks Inc., Natick, MA) using the method of Berglund et al. [23], as implemented in the ISMRM Fat-Water Toolbox [24], and using a 9-peak model for the lipid spectral peaks [25]. The water and fat images produced by the reconstruction were used to calculate the signal fat fraction (sFF), defined as sFF=fat/(fat+water). 20 vertebrae were imaged with adequate resolution and acceptable noise. Manual rigid registration was performed to anatomically match MRI and DECT/QCT ROIs.

### 2.6. *Ex vivo* analysis

Less than 12 hours after MRI imaging, the lumbar vertebrae, L1–L5, were removed, separated, and placed in formalin. Afterwards, 13 individual vertebrae were imaged using a Siemens Inveon® MicroCT at the Center for Magnetic Resonance Research at the University of Minnesota. The μCT parameters used included 1.3x magnification, 4 binning, 0.5 mmAl filter, and 80kVp to produce 95 μm/voxel images (Fig. 2b).

μCT DICOM images were analyzed using the BoneJ plugin [26] on ImageJ[27]. A threshold of approximately 0.8 grams hydroxyapatite/cc was used to separate out mineralized tissue. Manual rigid registration was performed to anatomically match microCT and DECT/QCT data. A region of interest similar to the DECT imaging was applied in identical locations of the lumbar vertebrae. Bone mineral content (BMC) and bone volume per total volume (BV/TV) were measured.

### 2.7. Statistical Analysis

Mean QCT-derived vBMD, MAT, and mcvBMD values were determined at 446 skeletal sites. To compare *in vivo* imaging results (i.e. QCT and DECT) to *ex vivo* imaging results (i.e. BMC and BV/TV), as well as to MAT results (i.e. DECT-derived MAT and MRI-derived sFF), spearman nonparametric correlation coefficients and two-tailed P value were were determined using Graph Pad Prism software (Version 6.02). Significance of within-donor differences in QCT-derived vBMD and mcvBMD were assessed by a paired t-test for each skeletal site.

## 3. Results

When comparing MAT between DECT and MRI, regions of interest of matching size were created in the vertebral bodies and anatomically placed in approximately identical locations using manual rigid registration. The sFF (i.e. the intensity of marrow fat as assessed by MRI) of 20 vertebral bodies were recorded. Between the 5 patients, the values ranged from 23% to 79% marrow fat. Variations within each individual lumbar spine were far less with an average difference of 14% between max and min sFF. DECT-derived MAT was shown to be highly correlated with sFF results ($r = 0.881$, $p < 0.0001$). There was no correlation identified between MAT, assessed by either MRI sFF or DECT, and mcvBMD ($r = 0.067$ and $= 0.261$, respectively, $p>0.3$). However, a significant inverse correlation was observed between MAT, assessed by either MRI sFF or DECT, and uncorrected vBMD ($r = -0.818$ and $= -0.86$, respectively, $p<0.0001$) (see Fig. 3a).

The results from *ex vivo* analysis revealed heterogeneous characteristics among the 13 lumbar samples. BV/TV values ranged from 3.1% to 15% and BMC ranged from 0.016 to 0.223 mg of hydroxyapatite. The BV/TV and BMC values for the 13 vertebrae were compared to the vBMD and mcvBMD values of the QCT and DECT, respectively. In Fig. 3b, a slightly better correlation with BV/TV is seen when vBMD is corrected for marrow composition than when assessed by QCT ($r = 0.545$, $p = 0.057$ and $r = 0.058$, $p = 0.850$, respectively). When BMC was correlated to DECT and QCT vBMD, there was a similar noteable difference ($r = 0.539$, $p=0.061$ and $r = 0.093$, $p=0.765$ respectively, Spearman correlation and two tailed p value estimation).

For the 23 skeletal sites, the average uncorrected vBMD using 140kVp QCT ranged from 783 mg/cm$^3$ to −44 mg/cm$^3$ (skull and proximal humerus, respectively). Fig. 4a compares these results to the marrow-corrected DECT dataset. QCT significantly overestimated the BMD for the vertebral bodies of the cervical and thoracic spine. By contrast, the BMD values were lower when assessed by QCT than by DECT in more caudal sites (e.g. tibia). At 14 of the 23 skeletal sites, the average difference between QCT-derived vBMD and

mcvBMD was significant at the $p < 0.05$ level (marked with * in Fig. 4a). MAT ratios at each skeletal site are shown in Fig. 4b, excluding the posterior occipital diploë due to large uncertainty with small marrow space. At sites with a higher ratio of yellow to red marrow, the difference between mean mcvBMD and vBMD had a high correlation with the mean marrow adiposity of each site ($r = 0.93$, $p < 0.0001$).

Higher marrow fat ratios were seen in proximal tibia and humerus. These two sites were also the only values that QCT determined to have a negative BMD (−11.9 and −44.3 mg/cc, respectively). Excluding the skull, the average (±SD) mcvBMD derived by DECT was 106 mg/cm$^3$ (±85.6 mg/cm$^3$) with the densest site being the talus (229 mg/cm$^3$). We also observed a gradual decline in mean mcvBMD in the axial skeleton from the top of the spinal column to the bottom (233 mg/cm$^3$ for C3; 93 mg/cm$^3$ for L5). Local differences in mcvBMD were also seen within individual bones such as the femur and tibia. Cancellous mcvBMD was lower in the proximal femur than the distal femur (40 mg/cm$^3$ and 62 mg/cm$^3$, respectively), and significantly lower ($p < 0.001$) in the proximal tibia than distal tibia (50 mg/cm$^3$ and 158 mg/cm$^3$, respectively).

## 4. Discussion

Traditionally, clinicians assess fracture risk by measuring areal BMD using DXA. However, DXA superimposes thick cortical with trabecular bone, and cannot quantify marrow fat. Since radiation therapy and chemotherapy cause rapid increases in marrow fat, uncorrected BMD measurements can lead to significant errors in BMD when measured by DXA or QCT. In this study, we imaged the entire skeleton *in vivo* and assessed marrow composition using DECT. A range of MRI sFF values (i.e. 23% to 79%), were used to validate the DECT modality for MAT assessment. We demonstrate that vBMD and MAT vary across skeletal sites. Additionally, we show that marrow fat, determined by either MRI sFF or DECT, is inversely correlated with vBMD when measured by QCT. This suggests an influence of MAT on uncorrected vBMD. We propose that DECT can be a useful imaging method to discern the adverse skeletal effects of cancer therapy. A more sensitive and accurate tool such as DECT might lead to greater understanding of the site-specific changes in fracture risk, such as greater risk of pelvic fractures after radiation therapy for gynecologic malignancy.

An increasing number of studies have investigated calcified cancellous tissue separate from marrow composition using high resolution imaging (e.g. peripheral quantitative computed tomography, micro-computed tomography (μCT), and quantitative ultrasound) [28–30]. However, their work is limited to *ex vivo* samples and peripheral skeletal sites. Poole et al. has established the importance of assessing 3D skeletal parameters for the evaluation of structural strength [31]. Another QCT-based study attempted to correct the vBMD results with microCT values [32]. However, both studies were not concerned with the influence of inherent marrow composition. The current work furthers the use of advanced CT techniques to simultaneously measure the metabolic changes in the two compartments of cancellous bone.

Our study adds to a growing body of knowledge by extending the observations to the entire skeleton *in vivo* and assess marrow composition using DECT (Fig. 1a). A method of assessing the two components of cancellous bone throughout the skeletal system might improve the ability to identify and monitor patients at high risk of fractures. A previous attempt to assess skeletal-wide heterogeneity of more metabolically-active (i.e. cancellous) bone was unable to separate adjacent skeletal regions, much less cortical from cancellous bone, due to technical limitations [33]. More recently, work by Frost et al.[3] and Yagi et al. [34] showed the functional heterogeneity of both osteoblastic activity and active marrow using $^{18}$F labeled FDG and NaF. Recent improvements in CT scanners, including dual energy, large bore, and larger couch travel, have permitted accurate and efficient investigations of cancellous bone throughout the whole body, including quantification of marrow fat [35, 36]. Correcting cancellous bone for MAT (i.e. mcvBMD) resulted with a moderate correlation to both BV/TV and BMC whereas no correlation was observed between either BV/TV or BMC and uncorrected vBMD. Therefore, using DECT to monitor bone health has advantages of being able to identify vBMD of calcified tissue while simultaneously characterizing marrow composition.

Although CT imaging increases radiation exposure to patients, whole body CT scans are already performed as part of a positron emission tomography (PET)/CT. Also, since radiation treatment planning CT scans are regularly given as part of the diagnosis, treatment and follow-up process, DECT could become very useful to the study of cancer survivors' bone health. To date, such images are taken with single energy CT and only used for anatomical referencing. Another benefit of whole body DECT would be for applications such as evaluating radiation dose from cancer treatment to the active marrow without assuming marrow composition from surrogate anatomy [37]. We expect these imaging studies to soon take advantage of reduced radiation exposure from DECT scans [38–40] and be able to monitor bone health.

### 4.1. Limitations

The present study was a feasibility study and did not have a high sample size. Although the correlation between DECT and MRI for MAT assessment is good, our study was limited in only validating regions with high marrow content, i.e. the lumbar vertebrae. We limited participants to subjects who had pre-arranged anatomical donation contracts with the University of Minnesota Bequest Program. Only Caucasian women were imaged, and cannot state whether skeletal heterogeneity would also exist in men or in other racial groups. Since we were performing a feasibility study, we did not restrict our cancer donors to those with a certain form of cancer, certain type of chemotherapy, or a standard dose or location of radiation therapy.

## 5. Conclusion

Bone mineral density and marrow composition vary among cancellous bone sites along the entire skeleton. With the ability to correct for marrow composition, DECT imaging of the entire human body can accurately assess the calcified vBMD of cancellous bone. The trend of cancellous vBMD among skeletal sites was similar for QCT and DECT. However,

marrow composition heterogeneity did reveal dynamic differences in some skeletal sites. Further validation with periphery skeletal sites would increase significance of DECT whole body assessment for bone health. These findings suggest potential for application in further prospective studies where accurate and longitudinal vBMD and marrow assessments are necessary (e.g. age related studies). This method could also be beneficial to longitudinal clinical studies where monitoring abscopal bone health changes in short time periods is desirable.

## Acknowledgments

This work was supported by the National Institute of Health grants (1R01CA154491-01; RO3 AR055333-02), National Institute of Child Health and Human Development (1K12-HD055887-01), the by the National Center for Advancing Translational Sciences of the National Institutes of Health Award Number 8UL1TR000114-02, and Cancer Center Support Grant P30 CA77398. Other grant support includes the Minnesota Medical Foundation and seed grants from the university (Academic Health Center, Grant in Aid, Masonic Cancer Center breast cancer research). Susanta K Hui is a scholar of the BIRCWH (Building Interdisciplinary Careers in Women's Health) program. This work was supported by Japan Society for the Promotion of Science Core to Core Program (23003). Karen Hansen serves as a medical monitor and consultant to Deltanoid Pharmaceuticals. All other authors have no conflicts of interest.

The authors wish to thank the women who donated their bodies for the advancement of education and research.

## References

1. Hui SK, Fairchild GR, Kidder LS, Sharma M, Bhattacharya M, Jackson S, Le C, Petryk A, Islam MS, Yee D. The Influence of Therapeutic Radiation on the Patterns of Bone Remodeling in Ovary-Intact and Ovariectomized Mice. Calcified Tissue International. 2013:1–13.
2. Yagi M, Arensten L, Shanley R, Rosen C, Kidder LS, Sharkey L, Yee D, Koizumi M, Ogawa K, Hui S. Whole Body Micro-PET/CT System Reveals Functional Heterogeneity and Early Local and Systemic Changes Following Targeted Radiation to the Murine Caudal Skeleton. Calcif Tissue Int. 2014 In Press.
3. Frost ML, Fogelman I, Blake GM, Marsden PK, Cook G Jr. Dissociation between global markers of bone formation and direct measurement of spinal bone formation in osteoporosis. J Bone Miner Res. 2004; 19:1797–804. [PubMed: 15476579]
4. Mitchell MJ, Logan PM. Radiation-induced changes in bone. Radiographics. 1998; 18:1125–36. quiz 1242–3. [PubMed: 9747611]
5. Bolotin HH, Sievanen H, Grashuis JL, Kuiper JW, Jarvinen TL. Inaccuracies inherent in patient-specific dual-energy X-ray absorptiometry bone mineral density measurements: comprehensive phantom-based evaluation. J Bone Miner Res. 2001; 16:417–26. [PubMed: 11204442]
6. Yu EW, Thomas BJ, Brown JK, Finkelstein JS. Simulated increases in body fat and errors in bone mineral density measurements by DXA and QCT. J Bone Miner Res. 2012; 27:119–24. [PubMed: 21915902]
7. Scheller EL, Rosen CJ. What's the matter with MAT? Marrow adipose tissue, metabolism, and skeletal health. Ann N Y Acad Sci. 2014; 1311:14–30. [PubMed: 24650218]
8. Scheller EL, Doucette CR, Learman BS, Cawthorn WP, Khandaker S, Schell B, Wu B, Ding SY, Bredella MA, Fazeli PK, Khoury B, Jepsen KJ, Pilch PF, Klibanski A, Rosen CJ, MacDougald OA. Region-specific variation in the properties of skeletal adipocytes reveals regulated and constitutive marrow adipose tissues. Nat Commun. 2015; 6:7808. [PubMed: 26245716]
9. Mazess RB. Errors in measuring trabecular bone by computed tomography due to marrow and bone composition. Calcif Tissue Int. 1983; 35:148–52. [PubMed: 6850397]
10. Kuiper JW, van Kuijk C, Grashuis JL, Ederveen AG, Schutte HE. Accuracy and the influence of marrow fat on quantitative CT and dual-energy X-ray absorptiometry measurements of the femoral neck in vitro. Osteoporos Int. 1996; 6:25–30. [PubMed: 8845596]

11. Gluer CC, Genant HK. Impact of marrow fat on accuracy of quantitative CT. J Comput Assist Tomogr. 1989; 13:1023–35. [PubMed: 2584480]
12. Rosen CJ, Ackert-Bicknell C, Rodriguez JP, Pino AM. Marrow fat and the bone microenvironment: developmental, functional, and pathological implications. Crit Rev Eukaryot Gene Expr. 2009; 19:109–24. [PubMed: 19392647]
13. Arentsen L, Yagi M, Takahashi Y, Bolan PJ, White M, Yee D, Hui S. Validation of marrow fat assessment using noninvasive imaging with histologic examination of human bone samples. Bone. 2015; 72:118–22. [PubMed: 25460181]
14. Hui SK, Arentsen L, Sueblinvong T, Brown K, Bolan P, Ghebre RG, Downs L, Shanley R, Hansen KE, Minenko AG, Takhashi Y, Yagi M, Zhang Y, Geller M, Reynolds M, Lee CK, Blaes AH, Allen S, Zobel BB, Le C, Froelich J, Rosen C, Yee D. A phase I feasibility study of multi-modality imaging assessing rapid expansion of marrow fat and decreased bone mineral density in cancer patients. Bone. 2015; 73:90–7. [PubMed: 25536285]
15. Graser A, Johnson TR, Bader M, Staehler M, Haseke N, Nikolaou K, Reiser MF, Stief CG, Becker CR. Dual energy CT characterization of urinary calculi: initial in vitro and clinical experience. Invest Radiol. 2008; 43:112–9. [PubMed: 18197063]
16. Christner JA, Kofler JM, McCollough CH. Estimating effective dose for CT using dose-length product compared with using organ doses: consequences of adopting International Commission on Radiological Protection publication 103 or dual-energy scanning. AJR Am J Roentgenol. 2010; 194:881–9. [PubMed: 20308486]
17. Hui SK, Arentsen L, Wilcox A, Shanley R, Yee D, Ghebre R. Spatial and temporal fracture pattern in breast and gynecologic cancer survivors. J Cancer. 2015; 6:66–9. [PubMed: 25553090]
18. Berger MJ, Hubbell JH, Seltzer SM, Chang J, Coursey JS, Sukumar R, Zucker DS. XCOM: Photon Cross Section Database. NIST Standard Reference Database. 1998; 8:87–3597.
19. Goodsitt MM, Hoover P, Veldee MS, Hsueh SL. The composition of bone marrow for a dual-energy quantitative computed tomography technique. A cadaver and computer simulation study. Invest Radiol. 1994; 29:695–704. [PubMed: 7960616]
20. Johnson TR, Krauss B, Sedlmair M, Grasruck M, Bruder H, Morhard D, Fink C, Weckbach S, Lenhard M, Schmidt B, Flohr T, Reiser MF, Becker CR. Material differentiation by dual energy CT: initial experience. Eur Radiol. 2007; 17:1510–7. [PubMed: 17151859]
21. Photon E. Proton and Neutron Interaction Data for Body Tissues. IRCU. 1992 Report 46.
22. Bolan PJ, Arentsen L, Sueblinvong T, Zhang Y, Moeller S, Carter JS, Downs LS, Ghebre R, Yee D, Froelich J, Hui S. Water-fat MRI for assessing changes in bone marrow composition due to radiation and chemotherapy in gynecologic cancer patients. J Magn Reson Imaging. 2013; 38:1578–84. [PubMed: 23450703]
23. Berglund J, Johansson L, Ahlstrom H, Kullberg J. Three-point Dixon method enables whole-body water and fat imaging of obese subjects. Magn Reson Med. 2010; 63:1659–68. [PubMed: 20512869]
24. Hu HH, Bornert P, Hernando D, Kellman P, Ma J, Reeder S, Sirlin C. ISMRM workshop on fat-water separation: insights, applications and progress in MRI. Magn Reson Med. 2012; 68:378–88. [PubMed: 22693111]
25. Hamilton G, Yokoo T, Bydder M, Cruite I, Schroeder ME, Sirlin CB, Middleton MS. In vivo characterization of the liver fat (1)H MR spectrum. NMR Biomed. 2011; 24:784–90. [PubMed: 21834002]
26. Doube M, Klosowski MM, Arganda-Carreras I, Cordelieres FP, Dougherty RP, Jackson JS, Schmid B, Hutchinson JR, Shefelbine SJ. BoneJ: Free and extensible bone image analysis in ImageJ. Bone. 2010; 47:1076–9. [PubMed: 20817052]
27. National Rasband WS. ImageJ. Bethesda, Maryland, USA: U.S. National Institutes of Health; 1997–2011.
28. Muller R, Hildebrand T, Hauselmann HJ, Ruegsegger P. In vivo reproducibility of three-dimensional structural properties of noninvasive bone biopsies using 3D-pQCT. J Bone Miner Res. 1996; 11:1745–50. [PubMed: 8915782]

29. Hazrati Marangalou J, Eckstein F, Kuhn V, Ito K, Cataldi M, Taddei F, van Rietbergen B. Locally measured microstructural parameters are better associated with vertebral strength than whole bone density. Osteoporos Int. 2014; 25:1285–96. [PubMed: 24306231]

30. Altuncu E, Akman I, Yurdakul Z, Ozdogan T, Solakoglu M, Selim N, Bilgen H, Ozek E, Bereket A. Quantitative ultrasound and biochemical parameters for the assessment of osteopenia in preterm infants. J Matern Fetal Neonatal Med. 2007; 20:401–5. [PubMed: 17674245]

31. Poole. Changing Structure of the Femoral Neck Across the Adult Female Lifespan. Journal of Bone and Mineral Research. 2009; 25:482–491.

32. Dall'Ara E, Varga P, Pahr D, Zysset P. A calibration methodology of QCT BMD for human vertebral body with registered micro-CT images. Med Phys. 2011; 38:2602–8. [PubMed: 21776797]

33. Bergmann P, Paternot T, Schoutens A. Regional measurement of bone calcium accretion rate and exchangeable pool with a whole-body counter: method and studies in subjects without bone disease. Calcif Tissue Int. 1983; 35:21–8. [PubMed: 6404530]

34. Yagi M, Arentsen L, Shanley RM, Rosen CJ, Kidder LS, Sharkey LC, Yee D, Koizumi M, Ogawa K, Hui SK. A dual-radioisotope hybrid whole-body micro-positron emission tomography/computed tomography system reveals functional heterogeneity and early local and systemic changes following targeted radiation to the murine caudal skeleton. Calcif Tissue Int. 2014; 94:544–52. [PubMed: 24562595]

35. Liu X, Yu L, Primak AN, McCollough CH. Quantitative imaging of element composition and mass fraction using dual-energy CT: three-material decomposition. Med Phys. 2009; 36:1602–9. [PubMed: 19544776]

36. Hui SK, Arentsen L, Sueblinvong T, Brown K, Bolan P, Ghebre RG, Downs L, Shanley R, Hansen KE, Minenko AG, Takhashi Y, Yagi M, Zhang Y, Geller M, Reynolds M, Lee CK, Blaes AH, Allen S, Zobel BB, Le C, Froelich J, Rosen C, Yee D. A phase I feasibility study of multi-modality imaging assessing rapid expansion of marrow fat and decreased bone mineral density in cancer patients. Bone. 2014; 73C:90–97.

37. Veres C, Allodji RS, Llanas D, Vu Bezin J, Chavaudra J, Mege JP, Lefkopoulos D, Quiniou E, Deutsh E, de Vathaire F, Diallo I. Retrospective reconstructions of active bone marrow dose-volume histograms. Int J Radiat Oncol Biol Phys. 2014; 90:1216–24. [PubMed: 25442047]

38. Yeh BM, Shepherd JA, Wang ZJ, Teh HS, Hartman RP, Prevrhal S. Dual-energy and low-kVp CT in the abdomen. AJR Am J Roentgenol. 2009; 193:47–54. [PubMed: 19542394]

39. Kerl JM, Bauer RW, Maurer TB, Aschenbach R, Korkusuz H, Lehnert T, Deseive S, Ackermann H, Vogl TJ. Dose levels at coronary CT angiography--a comparison of Dual Energy-, Dual Source- and 16-slice CT. Eur Radiol. 2011; 21:530–7. [PubMed: 20862476]

40. Noh J, Fessler JA, Kinahan PE. Statistical sinogram restoration in dual-energy CT for PET attenuation correction. IEEE Trans Med Imaging. 2009; 28:1688–702. [PubMed: 19336292]

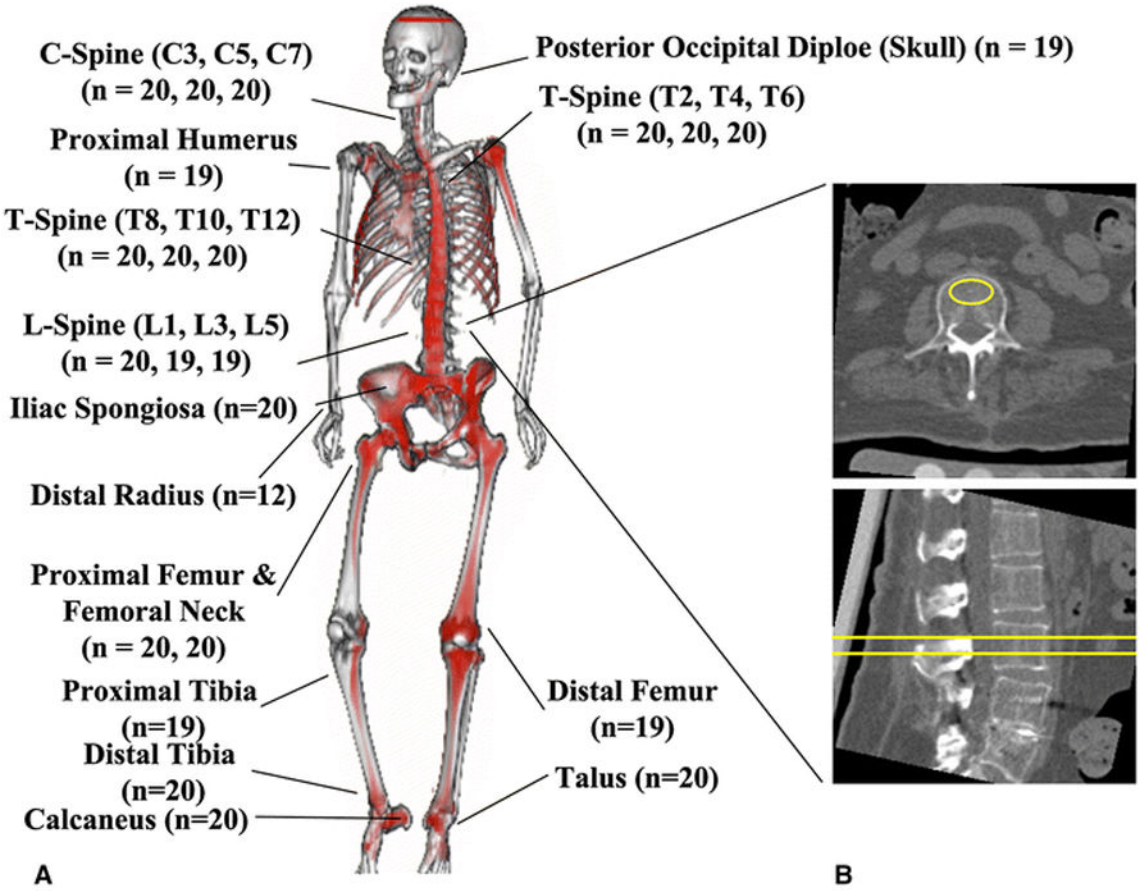


**Fig. 1.**

23 regions of interest representing areas of analyzed cancellous bone. a) First conceptual illustration of whole-body DECT image where less fatty marrow (i.e. more hematopoietically active) regions are highlighted in red and merged with a single energy CT skeletal contour. Apparent asymmetry caused by resampling limitations. b) Sample ROI placement for L3 (yellow)

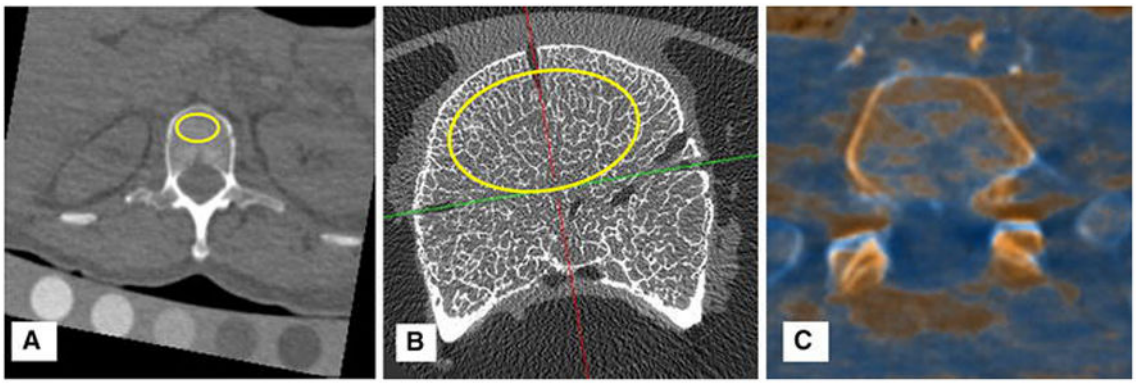


**Fig. 2.**

ROI placement (oval) for same L4 vertebral body in a) QCT image, b) μCT reconstruction, and c) DECT reconstruction highlighting areas of high marrow adiposity (maroon)

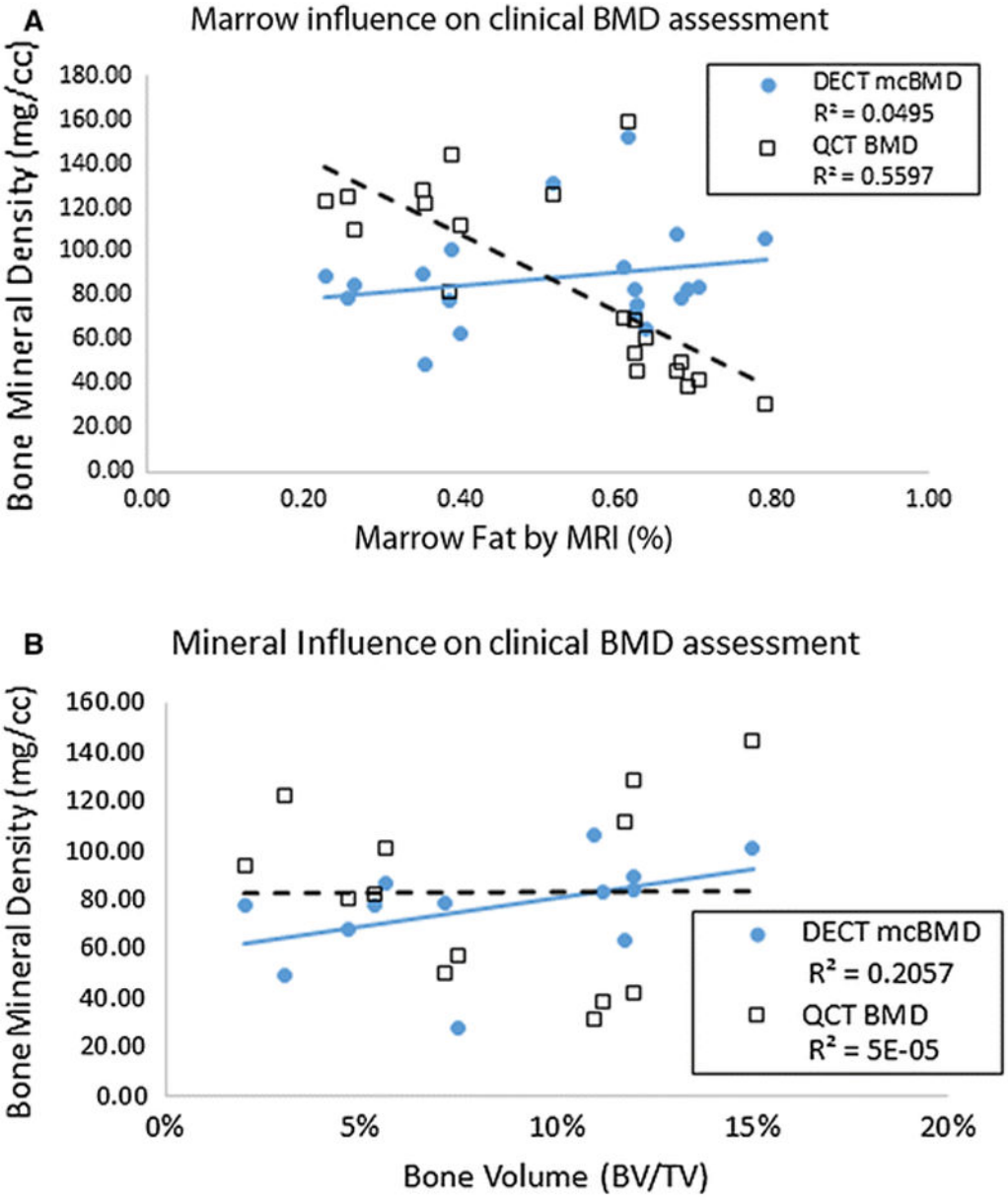


**Fig. 3.**

Marrow adiposity and mineral influences on *in vivo* imaging of cancellous bone a) percent of marrow adipose tissue (MAT) in marrow compartment assessed by MRI for 20 vertebral bodies. MAT is compared to volumetric BMD derived by marrow-corrected DECT and QCT. QCT-derived vBMD shows a significant inverse correlation with marrow fat than DECT-derived marrow corrected vBMD and b) *Ex vivo* analysis of bone volume to total volume (BV/TV) using μCT taken from 13 of the 20 vertebral bodies. Notice better correlation with BV/TV for DECT than QCT

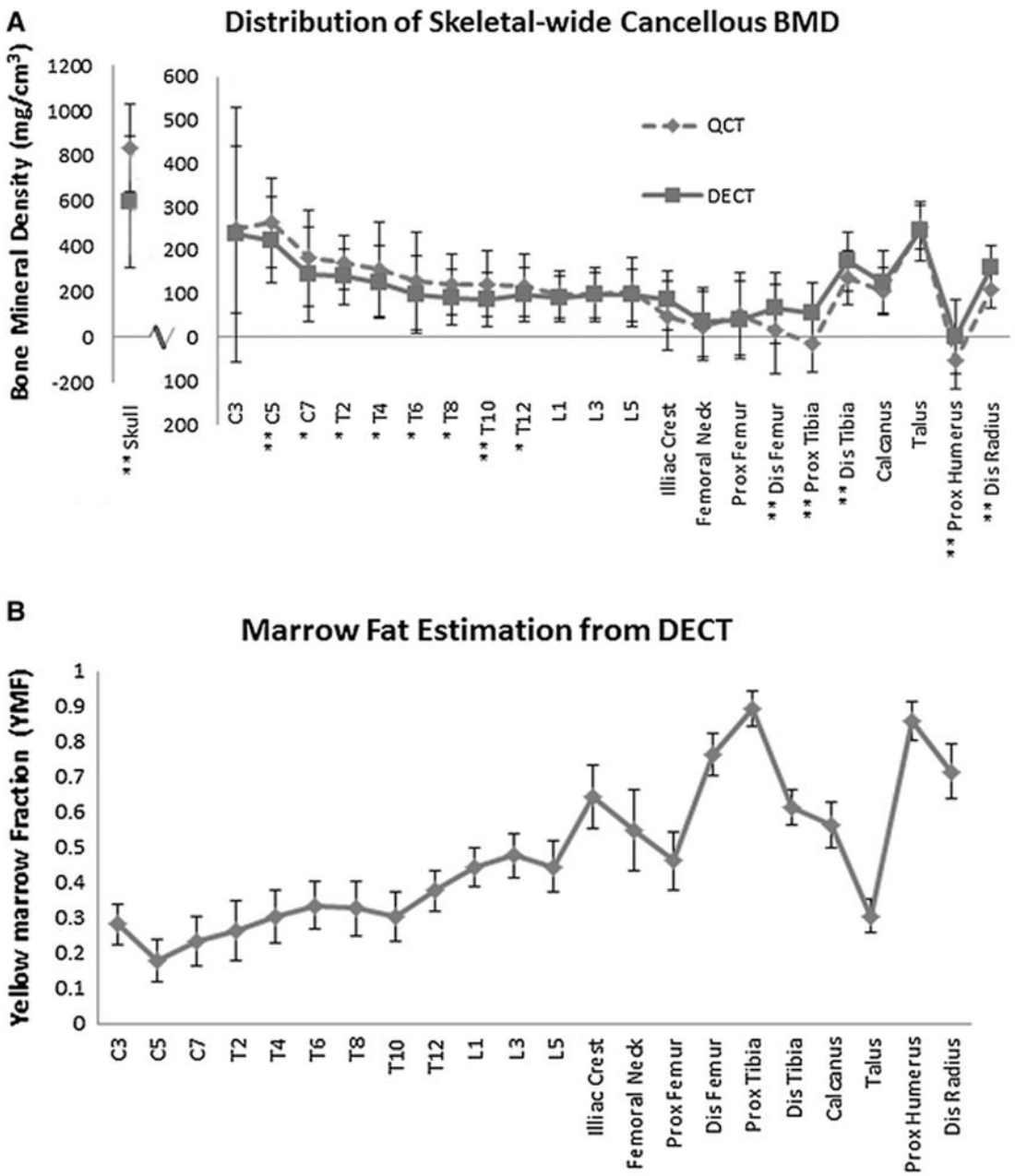


**Fig. 4.**

Distribution of cancellous bone throughout entire skeleton. Error bars are standard deviation for 20 female donors. a) Average Trabecular Bone Mineral Density distribution for 23 skeletal sites (skull separately). (* = $p<0.05$; ** = $p<0.01$). Notice lower BMD estimations in proximal tibia and humerus for QCT than DECT. b) Average Marrow fat (MAT) distribution from cervical spine to calcaneus